Environment International 191 (2024) 108986

Contents lists available at ScienceDirect

Environment International

journal homepage: www.elsevier.com/locate/envint

Full length article

Thirdhand smoke exposure promotes gastric tumor development in mouse and human

Chengfei Jiang [a,1], Lingyan Chen [a,1], Chunping Ye [b,1], Suzaynn F. Schick [c], Peyton Jacob III [d], Yingjia Zhuang [e], Jamie L. Inman [f], Changbin Chen [g], Lara A. Gundel [h], Hang Chang [f], Antoine M. Snijders [f], Xiaoping Zou [a,*], Jian-Hua Mao [f,*], Bo Hang [f,*], Pin Wang [a,e,*]

[a] Department of Gastroenterology, Affiliated Drum Tower Hospital, Medical School of Nanjing University, Nanjing, China
[b] Department of Obstetrics and Gynecology, Nanjing Maternity and Child Health Care Hospital, Women's Hospital of Nanjing Medical University, Nanjing, China
[c] Department of Medicine, Division of Occupational Environmental and Climate Medicine, University of California, San Francisco, CA 94143, USA
[d] Department of Medicine, Division of Cardiology, Clinical Pharmacology Program, University of California, San Francisco, CA 94143, USA
[e] Department of Gastroenterology, Nanjing Drum Tower Hospital, Clinical College of Nanjing Medical University, Nanjing, China
[f] Biological Systems and Engineering Division, Lawrence Berkeley National Laboratory, Berkeley, CA 94720, USA
[g] Shanghai Institute of Immunity and Infection, Chinese Academy of Science, Shanghai, China
[h] Indoor Environment Group, Energy Technologies Area, Lawrence Berkeley National Laboratory, Berkeley, CA 94720, USA

ARTICLE INFO

Handling Editor: Adrian Covaci

Keywords:
Thirdhand smoke (THS)
CC036 mice
Gene expression signature
Gastric cancer
Tumor-free survival
Epithelial-mesenchymal transition

ABSTRACT

The pollution of indoor environments and the consequent health risks associated with thirdhand smoke (THS) are increasingly recognized in recent years. However, the carcinogenic potential of THS and its underlying mechanisms have yet to be thoroughly explored. In this study, we examined the effects of short-term THS exposure on the development of gastric cancer (GC) *in vitro* and *in vivo*. In a mouse model of spontaneous GC, CC036, we observed a significant increase in gastric tumor incidence and a decrease in tumor-free survival upon THS exposure as compared to control. RNA sequencing of primary gastric epithelial cells derived from CC036 mice showed that THS exposure increased expression of genes related to the extracellular matrix and cytoskeletal protein structure. We then identified a THS exposure-induced 91-gene expression signature in CC036 and a homologous 84-gene signature in human GC patients that predicted the prognosis, with secreted phosphoprotein 1 (*SPP1*) and tribbles pseudokinase 3 (*TRIB3*) emerging as potential targets through which THS may promote gastric carcinogenesis. We also treated human GC cell lines *in vitro* with media containing various concentrations of THS, which, in some exposure dose range, significantly increased their proliferation, invasion, and migration. We showed that THS exposure could activate the epithelial-mesenchymal transition (EMT) pathway at the transcript and protein level. We conclude that short-term exposure to THS is associated with an increased risk of GC and that activation of the EMT program could be one potential mechanism. Increased understanding of the cancer risk associated with THS exposure will help identify new preventive and therapeutic strategies for tobacco-related disease as well as provide scientific evidence and rationale for policy decisions related to THS pollution control to protect vulnerable subpopulations such as children.

1. Introduction

Interactions between genes and environmental exposures shape health and disease (Mbemi et al., 2020). Among environmental exposures, cigarette smoke is particularly pernicious. It consists of mainstream smoke, directly inhaled by smokers, and secondhand smoke (SHS), which non-smokers inadvertently breathe in. Both contain many mutagenic and carcinogenic compounds, including N-nitrosamines,

Abbreviations: THS, thirdhand smoke; SHS, secondhand smoke; CC, collaborative cross; GC, gastric cancer; SPP1, Secretory Phosphoprotein 1; TRIB3, tribbles pseudokinase 3; TCGA-STAD, The Cancer Genome Atlas-Stomach Adenocarcinoma; EMT, epithelial-mesenchymal transition; ECM, extracellular matrix; LC–MS/MS, Liquid Chromatograph Mass Spectrometer/Mass Spectrometer; PCA, principal component analysis; PAH, polycyclic aromatic hydrocarbon.

* Corresponding authors at: Department of Gastroenterology, Affiliated Drum Tower Hospital, Medical School of Nanjing University, Nanjing, China (P. Wang).
E-mail addresses: zouxp@nju.edu.cn (X. Zou), jhmao@lbl.gov (J.-H. Mao), Bo_Hang@lbl.gov (B. Hang), pinwang729@gmail.com (P. Wang).

[1] Chengfei Jiang, Lingyan Chen and Chunping Ye share co-first authorship.

https://doi.org/10.1016/j.envint.2024.108986
Received 1 March 2024; Received in revised form 22 July 2024; Accepted 24 August 2024
Available online 26 August 2024

polycyclic aromatic hydrocarbons (PAHs), and volatile organic compounds, some of which have been conclusively linked to the development of lung cancer (Hecht, 2003; IARC, 2004; Office of the Surgeon General (US), 2004; CEPA, 2005; Hecht, 2012). SHS is a mixture of sidestream smoke, from the smoldering cigarette, and mainstream smoke exhaled by a smoker (IARC, 2004). The carcinogenic effects and underlying processes caused by SHS exposure are believed to be largely the same as those of mainstream smoke (Zhang et al., 2023; Dehghani et al., 2024). The concept of thirdhand smoke (THS) was identified as a new route of tobacco-related exposure. THS is the tobacco smoke residues that persist on indoor surfaces and in dust. This residue remains long after the smoke itself has dissipated, posing a constant exposure risk (Matt et al., 2011; Jacob et al., 2017). Very importantly, THS constituents may react with environmental pollutants to form secondary products (Destaillats et al., 2006; Sleiman et al., 2010). The harmful constituents of THS have the potential to re-enter indoor air environments leading to continued human exposure through inhalation, ingestion, and dermal contact. Moreover, THS residues are stubbornly resistant to standard cleaning techniques (Matt et al., 2021), presenting a health risk that is not easily mitigated.

Through the application of sophisticated molecular techniques, *in vitro* assays, and *in vivo* animal models, more than a hundred toxic substances have been identified in THS samples, many of which are recognized as carcinogens by the International Agency for Research on Cancer (IARC), including tobacco-specific nitrosamines (TSNAs, such as NNK, NNN and NNA), PAHs, and benzene (IARC, 2007; Jacob et al., 2017; Schick et al., 2014; Tang et al., 2022). Laboratory studies determined that even at low, environmentally realistic doses, THS exposure induces DNA strand breaks and oxidative stress in various human cell cultures (Hang et al., 2014; Hang et al., 2018; Bahl et al., 2016a, 2016b; Sarker et al., 2020; Tang et al., 2022; Sakamaki-Ching et al., 2022), including human bronchial epithelium cell line BEAS-2B (Hang et al., 2013) and human hepatocellular carcinoma cell line HepG2 (Hang et al., 2014; Hang et al., 2018) in our own studies, suggesting that THS is a risk factor for cancer development. Indeed, *in vivo* experiments in mouse models demonstrated that short-term THS exposure increased lung cancer rates in A/J mice (Hang et al., 2018; Hang et al., 2019a, 2019b). We have recently used the population-based Collaborative Cross (CC) mouse model to further investigate the role of host genetics on cancer risk associated with THS exposure (Yang et al, 2023). We showed that tumor susceptibility after THS exposure varied significantly across 8 different CC strains tested (Yang et al., 2023). The CC mouse system serves as a proxy for the genetic heterogeneity seen in the human population, making it an ideal model system for studying gene-environment interactions, as reported in our previous studies (Wang et al., 2019; Mao et al., 2015; Kim et al., 2019; Mao et al., 2020; He et al., 2021; Jin et al., 2021; Snijders et al., 2016).

Smoking tobacco is an important behavioral risk factor for gastric cancer (GC) development. Moreover, SHS has been associated with *H. pylori* infection and increased GC risk, especially in non-smoking females (Li et al., 2020). Our current research aims to elucidate the specific pathways and mechanisms by which THS contributes to GC risk using the CC036 mouse gastric tumor model, together with *in vitro* human gastric cell lines. Our findings provide significant insight into the gene-environment interaction in cancer etiology as well as help make smoking regulations associated with THS.

2. Materials and methods

2.1. THS sample generation and characterization

THS samples were generated on cotton terry cloth from a controlled laboratory system, which is described in our previous work (Hang et al., 2013). Briefly, the cloth samples were used as a substitute for indoor surfaces and were repeatedly exposed to fresh SHS in a 6-m^3 stainless steel chamber. During exposure, a total of 2795.6 mg of smoke particles was discharged into the chamber. This is equivalent to the smoke from 200 to 350 cigarettes over 2 years and 9 months, or approximately 1/5–1/3 of a cigarette per day. The THS cloth was vacuum-packed in Mylar film after exposure and stored at −20℃ until use.

For chemical analysis and cellular experiments, both THS-laden and clean cloth samples were weighed, cut into small pieces, and immersed in serum-free RPMI-1640 at a ratio of 0.1 g paper to 2 ml medium, then vortexed and centrifuged as previously described (Hang et al., 2013). For chemical analysis, 1 ml of media with THS and another without were taken out and stored at 4 °C until use. Targeted THS compounds in the RPMI 1640 samples were analyzed following the procedures described in the previous study (Hang et al., 2013), using liquid chromatography-tandem mass spectrometry (LC–MS/MS) as described in Whitehead et al. (Whitehead et al., 2015).

2.2. CC036 mouse strain and THS exposure

CC036 mice were obtained from the Systems Genetics Core Facility at the University of North Carolina (Welsh et al., 2012). At Lawrence Berkeley National Laboratory (LBNL), the cancer study was carried out in accordance with NIH IUCAC guidelines and the Animal Welfare and Research Committee at LBNL approved the animal use protocol for this study. CC036 mice were randomly divided into THS-exposed and unexposed (control) groups immediately after weaning. Mice were exposed to THS from 4 to 9 weeks of age as follows: a 10 × 10 cm^2 swatch (3.4 g) of THS-exposed or control terrycloth was added to the standard bedding in the cages, and the cloth swatches were replaced once a week during the standard cage change. The nicotine loading of the swatches was 23.4 μg/g for a total of 79.56 mg. This value is comparable to the ingestion exposure of a toddler estimated by Bahl et al. (Bahl and Jacob, 2014), In general, we aimed to apply environmentally relevant doses of THS exposure in our studies. Tumor development was monitored for a total of 18 months.

At Nanjing University Affiliated Drum Tower Hospital, primary gastric epithelial cells were isolated from stomach tissues obtained from CC036 mice (see details below). The Ethics Committee at this hospital approved the animal use protocol.

2.3. Post-mortem examination and histological assessment of THS-exposed CC036 mice

Upon reaching their experimental endpoint of the study period, both THS-treated and control CC036 mice were subjected to a thorough necropsy immediately after euthanasia (Yang et al., 2023). Tumors were located through direct observation, and their number, size, placement, and any metastases were documented. In instances where mice were discovered deceased before the end of the experiment (categorized as Found Dead in Cage, or FDIC), the timing of death was noted, along with any neoplastic findings during necropsy.

Tissue samples were preserved in 10 % formalin (Azer Scientific, USA) and were maintained at ambient temperature for 48 hrs. Subsequently, the fixed samples were rinsed and stored in 75 % ethanol at 4 °C. All collected tissues were then embedded in a paraffin medium, sectioned to a thickness of 4 μm, and stained with hematoxylin and eosin (H&E). This process was performed at the Histology and Biomarkers Core at the UCSF, Mt. Zion Campus in San Francisco. The stained tissues were then evaluated for histopathological changes.

2.4. Ths-exposure of CC036 primary gastric tumor epithelial cells and human GC cell lines

For the isolation of primary epithelial cells from CC036 stomach, gastric tissues were cut into small pieces. After 2 washes with antibiotics-containing PBS, tumor pieces were incubated with an enzyme cocktail made of collagenase II (400 U/ml, C2-BIOC, Sigma-Aldrich, USA) and DNaseI (350 U/ml, 10104159001, Roche, USA) for

30 min at 37 °C. The supernatant containing the cell suspension was removed and filled with DMEM-F12 medium (01–170-1A, Biological Industries, Israel) containing 10 % fetal bovine serum (FBS; 10099141C, Grand Island Biological Company, Australia). The remaining tissue was incubated with an enzyme cocktail for another 30 min at 37℃. Next, all cell suspensions were combined and filtered through a 70-μm cell strainer. After additional washes, cells were cultured, and the medium was renewed after 5 days and subsequently when necessary.

Two human GC cell lines AGS and MGC803 (Shanghai Institute of Biochemistry and Cell Biology, Shanghai, China), were cultured in RPMI-1640 medium (BC-M−017, Biochannel, China) containing 10 % FBS, penicillin–streptomycin (100 U/ml, 15140122, Grand Island Biological Company, USA). The cells were placed at 37℃ in a humidified incubator containing 5 % CO_2 (3131, Thermo Fisher Sientific, USA) and used for experiments after they reached 70–80 % confluence.

THS-RPMI-1640 was prepared as above and diluted in a complete culture medium at ratio of 1:20, 1:80 and 1:160, respectively. Cells were treated with fresh THS or control culture medium for 24 hrs before subsequent experiments. Each experiment was repeated at least 3 times, with 3 wells each time.

2.5. Transcriptome profiling of CC036 primary cells

At 24 hrs after THS treatment, total RNA from CC036 primary epithelial cells was extracted using the TRIzol® reagent (15596018, Invitrogen, USA) for high-throughput RNA sequencing. The library construction and sequencing were conducted by GENEDENOVO following standard protocols for next-generation sequencing. RNA integrity was confirmed prior to sequencing. Subsequent bioinformatics analysis was performed with STAR v2.5.2b (Alexander Dobin, (c) 2009–2024) to align reads to the human reference genome (GRCh38), including necessary components as per the 1000 Genomes Project. The quantification of gene expression levels was performed using HTSeq 0.6.1p2 (Simon Anders, European Molecular Biology Laboratory (EMBL), (c) 2010.) against the Gencode v26 primary assembly annotations. Differential gene expression analysis was carried out using DESeq2 v1.40.2. Significant genes were identified based on a threshold of an absolute log2 fold change greater than 1 and a false discovery rate (FDR) below 0.05. A total of 91 differentially expressed genes were identified and intersected across varying concentrations of THS treatment. Functional annotation and enrichment analysis of the identified genes were performed using the clusterProfiler package v4.8.2. Visualization of expression patterns across samples was facilitated through heatmap representations, leveraging the gplots v3.0.1 R package.

2.6. Survival analysis of samples with THS-related expression patterns in TCGA-STAD

The differentially expressed genes were aligned with the human genome to identify human THS-related differentially expressed genes (N=84). We procured a dataset (N=409) from the TCGA-STAD project available on cBioPortal (https://www.cbioportal.org/). The 409 samples in the TCGA-STAD project were obtained from 22 clinical centers in the USA. The patients' racial backgrounds included Asian, White, and Black/African Americans. In addition, we used the online tool KMPlot and TNMplot to conduct some other analyses where all public available datasets were pooled and used for analyses. After filtering out genes with missing values, we applied the ConsensusClusterPlus package (version: 3.18) to perform consensus clustering of the samples using the Spearman method for distance calculation (kmdist), stratifying the samples into two groups. To compare the survival outcomes between the two groups, Kaplan-Meier plots were generated using the survminer package (version 0.4.9), and statistical significance was assessed using the log-rank test. This comparison allowed us to analyze the survival patterns associated with THS-related gene expression within the GC patients in the TCGA-STAD database.

2.7. Multiplex immunohistochemistry in mouse tissue using Opal-TSA fluorophores

To evaluate the effects of THS exposure on the immune microenvironment in gastric tumor in THS-treated or control CC036 mice, a multiplexed immunohistochemical approach was employed utilizing fluorescent tyramine signal amplification reagents from PANO 7-plex IHC Kit (10082100100, Panovue, China), designed for the sequential application and removal of primary and secondary antibodies, while selectively preserving the fluorescent signals of bound antigens until all target molecules were fluorescently labeled. For the preparation of the tissue sections, paraffin-embedded samples underwent xylene and graded ethanol deparaffinization followed by antigen retrieval. Endogenous peroxidase activity was inactivated (SP KIT-A1, Fuzhou Maixin Biotech, Fuzhou, China), and non-specific antibody binding was precluded with an appropriate blocking buffer (SP KIT-B1, Fuzhou Maixin Biotech, Fuzhou, China). Primary antibody incubation involved the following: anti-CD3 (17617–1-AP, Proteintech, China, 1:500 dilution), anti-CD4 (ab183685, Abcam, USA, 1:1000 dilution), anti-CD8α (98941, Cell Signaling, USA, 1:400 dilution), anti-FoxP3 (12653, Cell Signaling, USA, 1:400 dilution), and anti-pan-Cytokeratin (NB600-579, Novus, USA, 1:100 dilution). The secondary detection utilized Opal polymer HRP-conjugated anti-rabbit antibodies ·from PANO 7-plex IHC Kit, followed by incubation with one of the designated Opal fluorophores-PPD 520, PPD 540, PPD 570, PPD 620, or PPD 690 (1:100 dilution from PANO 7-plex IHC Kit)—in accordance with the manufacturer's protocol. Sections were mounted in SlowFade Gold Antifade Reagent with DAPI (Thermo Fisher Scientific). For comprehensive tissue analysis, slides were scanned at 10x magnification utilizing the Vectra Polaris System (Vectra 3, Akoya Biosciences, USA). The gathered data was analyzed using the Inform 2.6.0 software suite (Akoya Biosciences, USA).

2.8. Immunohistochemistry analysis of human GC tissues

After obtaining the patient consent, tissue sections from 10 GC patients were obtained from the Department of Pathology, the Affiliated Drum Tower Hospital of Nanjing University. This study received approval from the Research Ethics Committee at Nanjing Drum Tower Hospital (document number: 2023–614-01). Written informed consent was secured from every participant. All procedures involving clinical samples were conducted in strict adherence to the tenets of the Declaration of Helsinki.

Paraffin-embedded tissues were sectioned to 5 μm-thick slices followed by deparaffinization in xylene and graded ethanol, then antigen retrieval via microwave heating. We used a proprietary solution (SP KIT-B1, Fuzhou Maixin Biotech, Fuzhou, China) to inhibit endogenous peroxidase activity and a blocking buffer from the same company to prevent non-specific antibody binding (SP KIT-A1, Fuzhou Maixin Biotech, Fuzhou, China). The slices were incubated with primary antibodies against Osteopontin (22952–1-AP, Proteintech, China, 1:200 dilution) and TRIB3 (13300–1-AP, Proteintech, China, 1:100 dilution) at 4 °C overnight. Subsequently, we used the UltraSensitive™ SP (Rabbit) IHC Kit (KIT-0105R, Fuzhou Maixin Biotech, China), following the manufacturer's protocol. After counterstaining with hematoxylin and mounting with neutral balsam, the stained sections were evaluated by two experienced pathologists. The assessment was based on the proportion of cells displaying staining intensity and a scoring system (1 = low positive; 2 = moderate positive; 3 = strong positive). The IHC score was calculated using the formula:

$$\text{IHC score} = \Sigma\,(\text{proportion of stained intensity cells} \times \text{staining intensity score})$$

2.9. Bioinformatics

To ascertain the association between *SPP1* and *TRIB3* expression and

overall survival (OS) in GC patients, we utilized the Kaplan-Meier Plotter through the K-M Plotter tool (available at https://kmplot.com/analysis/) to conduct survival curve analyses.

The TNMplot platform offers a detailed examination of Gene chip data, facilitating the investigation of gene expression in specific tissue types (available at https://www.tnmplot.com). In our study, we assessed the differential expression patterns of *SPP1* and *TRIB3* between normal and gastric tumor tissue samples.

2.10. Statistical analysis

The experiments were independently replicated a minimum of three times to ensure reliability. Data analysis was conducted using SPSS software (version 19.0, IBM Corp.). Results are expressed as mean values ± standard error of the mean (SEM) from these replicates. To ascertain the statistical differences between datasets, one-way ANOVA was utilized, followed by the Tukey post hoc test for multiple comparisons. A p-value of less than 0.05 was considered statistically significant, with levels of significance denoted as follows: $*p < 0.05$, $**p < 0.01$, and $***p < 0.001$.

3. Results

3.1. THS exposure promotes gastric adenocarcinoma development in CC036 mice

To study the effect of THS on the development of gastric tumor, we reanalyzed the data in CC036 mice from our previous study (Yang et al., 2023), where CC036 mice were exposed to standard bedding supplemented with THS-terrycloth or to standard bedding only, by focusing on gastric tumor occurrence and free survival analysis. As shown in Fig. 1**A**, exposure to THS significantly reduced gastric tumor-free survival time in CC036 mice exposed to THS ($p < 0.05$). Exposure to THS significantly increased the gastric tumor rate as we previously described (Yang et al., 2023) (Fig. 1**B**) and the histopathological analysis revealed that majority of tumors occurred were adenocarcinoma (Fig. 1**C**).

We also assessed the effects of THS exposure on the immune microenvironment in gastric adenocarcinoma from THS-treated or control CC036 mice using multicolor immunofluorescence analysis. As shown in Supplementary Fig. 1A, we observed the distribution and proportion of T-helper cells (CD3+/CD4+), T-suppressor cells (CD3+/CD8+), Treg cells (CD4+/FoxP3+), and tumor epithelial cells (PanCK+) in GC tissue sections of CC036 mice in both THS-exposed and control groups, and no significant differences were found between these two groups (Supplementary Fig. 1). Supplementary Fig. 2 showed that there was no significant difference in the infiltration of immune cells and macrophages in the tumor tissues of the THS-exposed group compared to the control group. These findings collectively suggest that there is no statistically significant difference in the tumor immune microenvironment between THS-treated and control groups.

3.2. THS exposure enhanced the function of genes related to ECM and cytoskeletal protein structures in primary CC036 gastric epithelial cells

To delineate the molecular mechanism for the contribution of THS exposure to gastric tumor development, we treated primary gastric epithelial cells isolated from CC036 mice with different dilutions of THS in cell culture medium or control medium for 24 hrs, RNA was isolated from these cells for sequencing. Principal component analysis (PCA) revealed a distinct separation among the groups, with control samples clustering tightly, suggesting minimal variability within the untreated cells. Conversely, the THS-treated samples display a distinct divergence from the controls along the second principal component (PC2) (Fig. 2**A**). This separation reflects significant changes in gene expression profiles attributable to THS treatment.

Differentially expressed genes (DEG) analysis was carried out to assess the transcriptional impact of varying THS concentrations. Interestingly, gene expression changes were most pronounced in the 1:160 dilution group, followed by the 1:80 dilution group, with least in the 1:20 dilution group. The comparison between the 1:160 dilution group

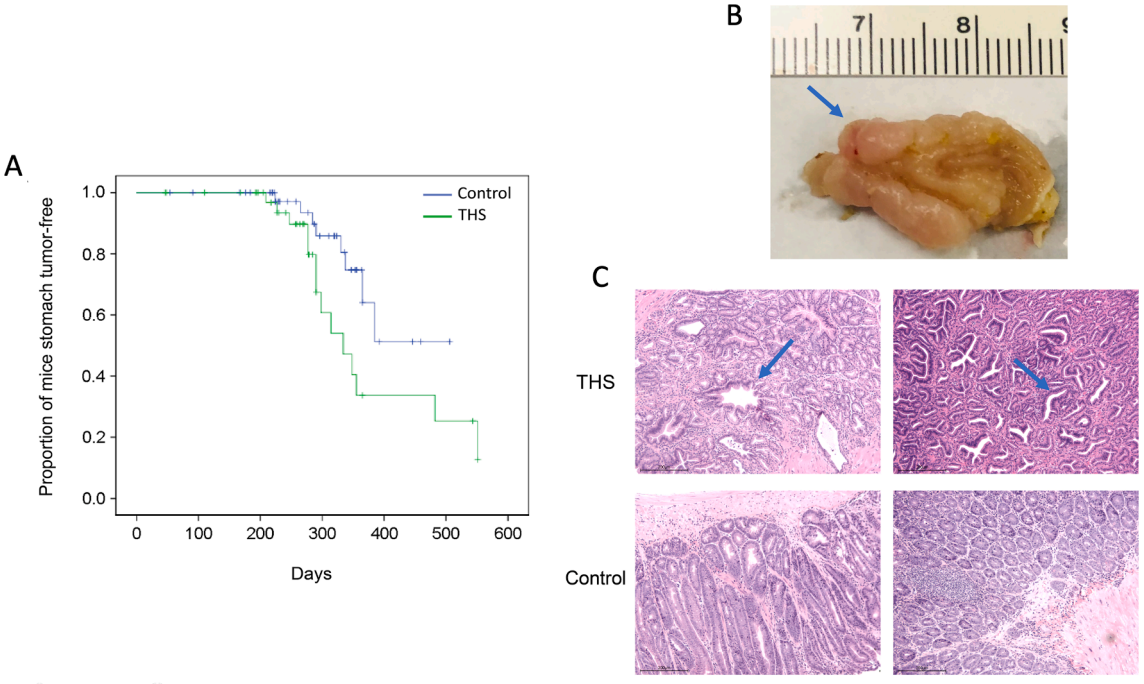

Fig. 1. Impact of THS exposure on GC incidence and tumor-free survival in CC036 mice. (A) Kaplan-Meier curves depicting tumor-free survival (TFS) in control (blue) and THS-exposed (green) cohorts, with statistical significance determined via the log-rank test; (B) Representative photograph of a gastric tumor in a CC036 mouse; (C) Histopathological analysis of gastric tumors from THS-exposed and control CC036 mice, visualized with H&E staining (100 × magnification). (For interpretation of the references to colour in this figure legend, the reader is referred to the web version of this article.)

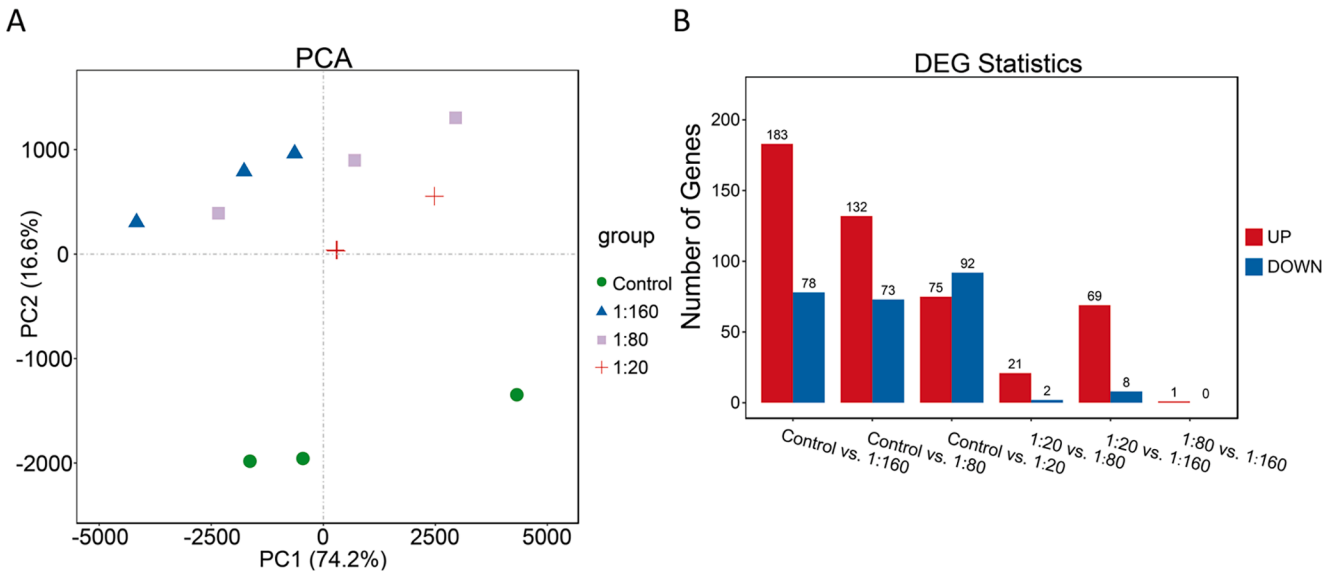

Fig. 2. Transcriptional impact of varying THS concentrations profiled by RNA sequencing. (A) PCA of RNA sequences confirms significant transcriptional changes associated with different THS gradients (1:160, 1:80, 1:20); (B) A bar graph illustrating the count of significantly upregulated and downregulated genes between control and THS-treated groups.

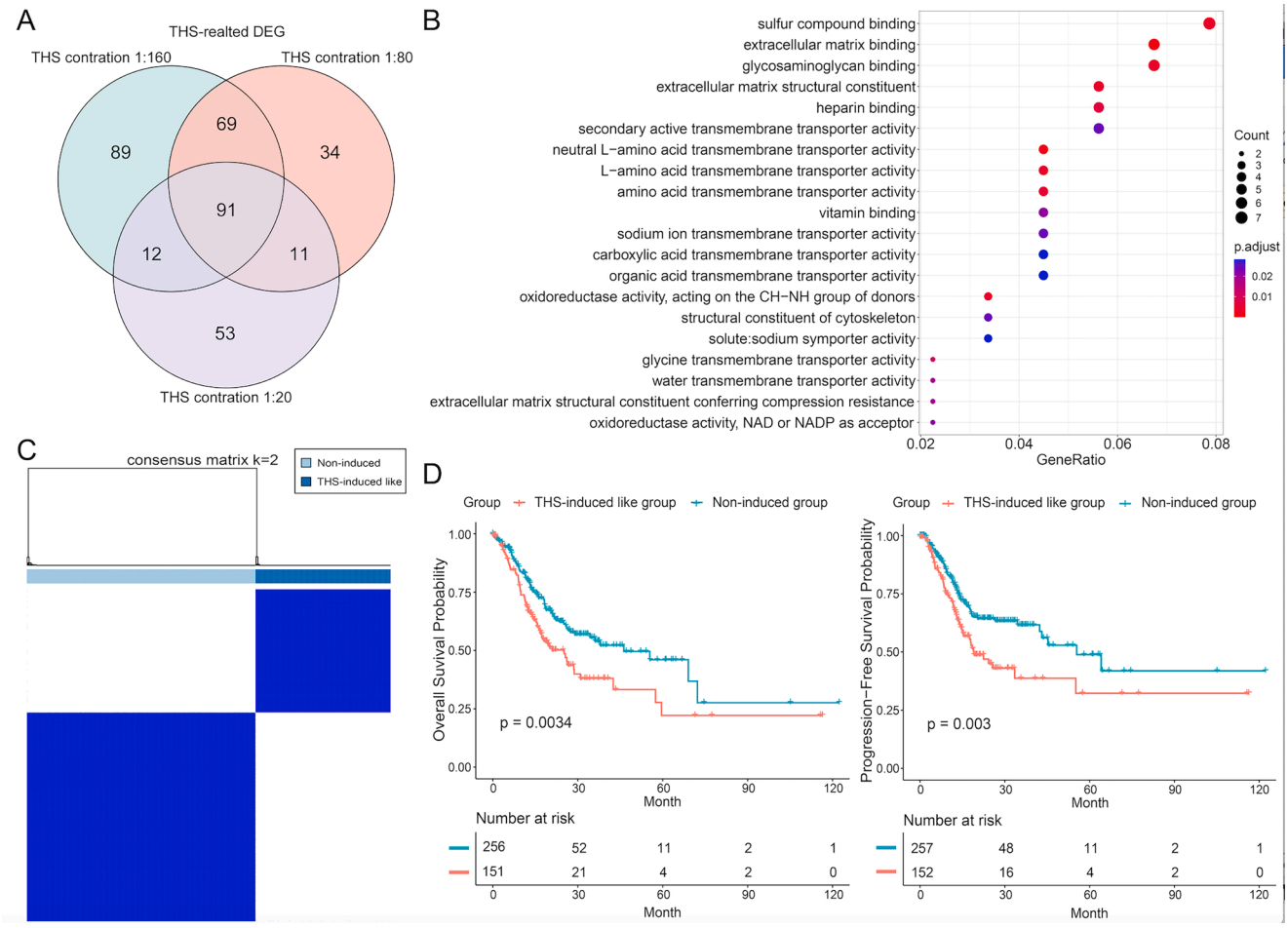

Fig. 3. Correlation of THS-induced DEGs with ECM and cytoskeletal development in CC036 mice and prognostic relevance in human GC patients. (A) A Venn diagram showing 91 DEGs shared across 1:160, 1:80, and 1:20 dilution groups compared to the control; (B) Gene Ontology (GO) analysis elucidating the molecular functions of the 91 THS-related DEGs; (C) Application of K-means consensus clustering to separate 409 TCGA-STAD samples into THS-related and non-THS groups, based on the 84 THS-related gene expression profiles; (D) Kaplan-Meier plots comparing OS and PFS between the THS-induced-like and non-induced groups. The P-values were derived from the log-rank test.

and the control group showed 183 genes upregulated and 78 genes downregulated. The 1:80 dilution group had 132 genes upregulated and 73 genes downregulated. In the 1:20 dilution group, there were 92 genes upregulated and 75 genes downregulated (Fig. 2**B**). These findings suggest that the effects observed at the 1:160 dilution level are the most pronounced among the three concentrations, potentially indicating a dose-dependent response in gene expression modifications upon THS exposure. Compared to the control group, we observed a total of 91 genes that consistently changed their expression in the primary gastric epithelial cells across three different concentration gradients of THS (adj. P<0.05 and fold-change >|2|; Fig. 3**A**, Supplementary Table S1).

Enrichment analysis indicated that the functions of the above 91 genes are primarily associated with sulfur compound binding, extracellular matrix binding, and extracellular matrix structure binding, linking them closely with the structure and function of the ECM and cytoskeletal proteins (Fig. 3**B**, Supplementary Fig. 3).

3.3. Evaluation of the prognostic impact of a differentially expressed 84-gene signature in human gastric cancers

We further addressed whether the THS exposure-related 91-gene signature is associated with overall survival in human gastric cancer patients. We identified 84 human homologs of the 91 mouse genes. Using K-means consensus clustering, we divided 409 stomach adenocarcinoma samples from the TCGA-STAD database into two groups based on the expression levels of the 84 THS exposure-related genes. Based on their expression levels, we assigned one group as THS exposure-related group and the other one as the non-THS exposure group (Fig. 3**C**). Kaplan-Meier survival analysis combined with a log-rank test revealed that the prognosis of gastric cancer patients in the THS exposure-related group was significantly worse than that in the non-THS exposure group (Fig. 3**D**). These findings point to the fact that the THS gene signature identified in our study is associated with poor survival, providing further evidence for a link between THS exposure and GC development at the gene level.

3.4. SPP1 and TRIB3 may be targets in THS-promoted GC

SPP1 and *TRIB3* are increasingly recognized for their roles in digestive system tumors. In Fig. 4**A,** the expression levels of the two genes are represented using normalized Fragments Per Kilobase of transcript per Million mapped reads (FPKM).

$$\mathrm{FPKM(gene\,A)} = \frac{10^6 C}{NL10^3}$$

In the formula, C represents the number of sequencing reads mapped to gene A, and N represents the total number of sequencing reads mapped to the reference genome, and L is the number of base pairs in gene A. Of the human 84-gene signature related to THS exposure, *SPP1* and *TRIB3* expression levels were most significantly elevated in cells treated with a THS-containing medium at a 1:160 concentration ($p = 0.0013$, $p = 0.0002$;). We further confirmed that THS treatment increased protein levels of SPP1 and TRIB3 in the CC036 primary gastric epithelial cell line, as well as in the human AGS and MGC803 GC cell lines (Fig. 4**B**), consistent with the elevated transcriptional levels of the two genes by RNA-seq. Analysis of *SPP1* and *TRIB3* gene expression levels using TNMplot indicated that their transcriptional expression levels were higher in tumor tissues compared to normal tissues (p = 2.71e–121, p = 8.23e–11; Table 1 and Fig. 4**C**). We further validated increased expression of SPP1 and TRIB3 in human GCs by staining 20 pairs of tumors and peritumor samples, confirming higher levels of SPP1 and TRIB3 in the human GC tumor samples (Fig. 4**D**). To further assess the significance of *SPP1* and *TRIB3* in GC development, Kaplan-Meier analysis indicated that the expression levels of *SPP1* and *TRIB3* significantly affect the overall survival (OS) of GC patients (*SPP1*: HR=2.23, Logrank P=3.1e-14; *TRIB3*: HR=1.52, Logrank P=1.1e-05) (Fig. 4**E**). Collectively, these findings suggest that both *SPP1* and *TRIB3* play a role in GC development, and they may serve as targets through which THS exposure leads to poorer patient prognosis.

3.5. THS exposure influences in vitro tumorigenic traits in both mouse and human cells

3.5.1. Effects of THS exposure on cell migration and invasion

As shown in Fig. 5**A** immunofluorescence staining, the primary gastric cells we extracted from CC036 mice expressed the epithelial marker CK18 and barely expressed a mesenchymal marker, vimentin, indicating that these cells are epithelial origin (CK+/vimentin-). Using the transwell assay shown in Fig. 5**B**, we observed a significant increase in the number of cells traversing the chambers after treatment with THS extract at 1:160 and 1:80 for 24 hrs, demonstrating that THS exposure enhances the migration of the primary gastric epithelial cells. For human GC cell lines AGS and MGC803, we found that THS exposure (1:160, 1:80 and 1:20) significantly increased migration in both cell lines under no Matrigel culture condition (Fig. 5**. C-D**). Furthermore, THS exposure (1:160) also significantly enhanced cell invasion in both cell lines (Fig. 5**E-F**). Therefore, THS exposure significantly enhances cell migration and invasion in a dose-dependent manner.

3.5.2. THS exposure increases in vitro clonogenic growth

We next investigated whether a 24-hr THS exposure could increase clonogenic growth *in vitro*. As shown in Fig. 6, compared to the controls, the total number of colonies of AGS cells treated with THS (1:160, 1:80, 1:20) significantly increased (Fig. 6**A**). However, THS extract did not affect the clonogenic potential of the MGC803 cells (Fig. 6**B**). We speculate that the genetic component of MGC803 influences its sensitivity to THS exposure.

Next, we selected AGS cells for further soft agar assay for THS exposure-induced anchorage-independent growth. After three weeks of culture, the living cell clusters in agar were stained with NBT, and the diameters of five randomly selected cell clusters were measured under a microscope for each group. As shown in Fig. 6**C**, THS exposure (1:160) increased the diameter of colonies formed by AGS cells. Collectively, we concluded that THS exposure promotes oncogenic traits of the cell lines tested, but not universally, possibly dependent on genetic conditions.

3.5.3. THS exposure enhances anti-apoptotic capabilities in human GC cell lines

As depicted in supplementary Fig. 4A**, a** higher concentration (1:20) of THS exposure increased the proportion of apoptotic cells in AGS, while at lower concentrations (1:80, 1:160) of THS exposure reduced the proportion of apoptotic cells compared to untreated cells. However, THS exposure did not significantly alter the proportion of apoptotic cells in the MGC803 cell line (supplementary Fig. 4B). These results are consistent with the outcomes of the colony formation assays. In contrast, we observed no significant effect of THS exposure on the distribution of cells across the cell cycle in GC cell lines (Supplementary Fig. 5).

3.6. THS exposure activates the epithelial-mesenchymal transition (EMT) pathway

Given the RNA-seq results suggesting a functional enrichment of genes associated with cytoskeleton, adhesion, and other functions in THS-exposed CC036 gastric epithelial cells and considering the significant impact of THS exposure on cell invasion and migration, it is reasonable to speculate that THS exposure might activate the EMT pathway, thereby affecting the malignant phenotype of tumor cells. We then examined changes in the expression of representative genes in this pathway in the AGS and MGC803 cell lines. After a 24-hr treatment with 1:160 THS extract, qRT-PCR confirmed that the mRNA expression levels of *CTNNB1*, *TWIST1*, *CDH2*, *ZEB1*, and *ZEB2* were upregulated in THS-

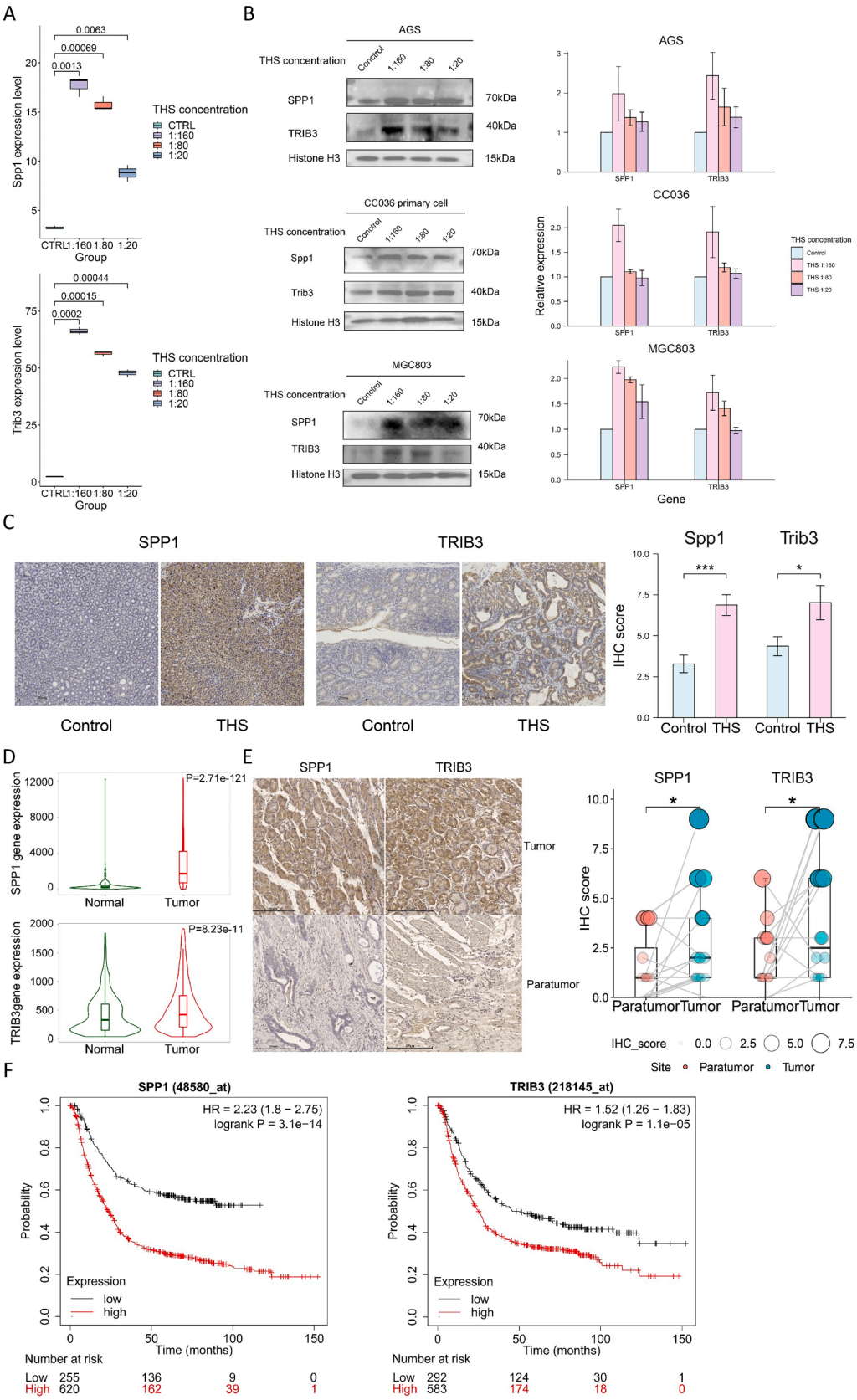

Fig. 4. Impact of THS exposure-upregulated genes *SPP1* and *TRIB3* on GC. (A) RNA sequencing profiles of *SPP1* and *TRIB3* expression in primary gastric cells of CC036 mice across THS gradients (1:160, 1:80, 1:20). (B) Protein levels of SPP1 and TRIB3 in MGC803, AGS, and CC036 primary gastric cell lines treated with THS. (C) TNM plot analysis using the online TNMplot web tool https://www.tnmplot.com/ showcasing *SPP1* and *TRIB3* expression. (D) IHC detection of SPP1 and TRIB3 in 20 GC tissues with paired paratumor tissue, with representative images (200 × magnification). (E) IHC detection of SPP1 and TRIB3 in GC tissues from 9 CC036

mice exposed to THS and 15 unexposed CC036 mice, with representative images (200 × magnification). (F) Kaplan-Meier plot analysis correlating *SPP1* and *TRIB3* expression with GC patient outcomes.

Table 1
TNM Plot Analysis Reveals Elevated Expression in Tumor Tissues Compared to Normal Tissues from Gene Chip Data.

Min	17	38	41	38
Q1	172.5	797	152	222
Med	260	2060	341	470
Q3	439	5445	617.5	902
Max	12,272	37,717	2847	5267
Upper whisker	815	12,374	1285	1920
N	360	1221	360	1221

exposed MGC803 cells (Fig. 7**A**). Similar findings were observed in AGS cells, where mRNA levels of *CTNNB1*, *SNAI1*, and *ZEB1* were overexpressed in THS-exposed AGS cell lines (Fig. 7**B**). Western blot results in MGC803 (Fig. 7**C**) and AGS (Fig. 7**D**) cell lines revealed a significant increase in the protein levels of the two EMT transcription factors, Twist1 and Snail, upon THS exposure, with the highest levels at a concentration of 1:160, which is consistent with increased invasion and migration observed in this study. These findings indicate that THS exposure activates the EMT pathway during the GC oncogenesis.

4. Discussion

This study is the first exploration of the mechanisms by which THS exposure causes GC. Many epidemiological studies have confirmed that both active and passive smoking are risk factors for GC (Steevens et al., 2010; Duan et al., 2009). Our recent *in vivo* studies have revealed that THS exposure promotes the development of GC in the CC036 mouse gastric tumor model (Yang et al., 2023). To assess the mechanisms by which THS causes GC, we selected the CC036 strain based on its demonstrated sensitivity to THS in the above publication (Yang et al.,2023) and conducted molecular and cellular studies using THS-exposed primary gastric epithelial cell lines from the CC036 mice and two human GC cell lines.

As previously mentioned, we used the CC mouse system, including the CC036 strain, to identify genetic variations associated with various phenotypes (Yang et al 2023 and refs therein). This mouse model offers distinct advantages for exposure studies because the genetic background of the host and THS exposure are well-controlled, which avoids the confounding effects of additional SHS exposure characteristic of human THS exposures. Our earlier studies have discovered that the CC036 mouse strain is prone to spontaneous GC (Wang et al., 2019). Therefore, we considered that CC036 would be a sensitive mouse model for the proposed THS exposure study in GC development.

We next subjected the primary gastric epithelial cells isolated from CC036 mice to different concentrations of THS and performed RNA sequencing to identify genes that might be involved in THS-promoted gastric carcinogenesis. We first identified 91 mouse genes with consistently and significantly altered expression across all THS concentrations, which were strongly enriched in sulfur compound binding, extracellular matrix binding, and ECM structure binding proteins implicating a close association with the ECM and structural function of cytoskeletal proteins. Dysregulation of ECM composition, structure, and other properties is associated with invasive cancer (Bonnans et al., 2014). By identifying the 84 human orthologous genes of the 91 mouse genes associated with THS exposure, we further build a molecular bridge to explore the possible impact of THS exposure on the occurrence of GC in humans. Kaplan-Meier survival curve analyses of patient cohorts revealed that the patients whose gene expression changes were similar to the THS exposure-related group had significantly worse prognosis, as compared to the other patients. This supports the hypothesis that THS exposure alters gene expression and may lead to a more invasive GC phenotype. This gene signature could serve as a tool for risk assessment, potentially guiding targeted monitoring and the development of personalized treatment plans for those patients demonstrating THS exposure-induced gene expression patterns.

Additionally, we note that of the 84 genes, 10 genes (ALDH1L2, ASNS, BCAT1, CA6, CHAC1, CTH, FUT1, GPD2, MTHFD2 and P4HA3) are involved in metabolic pathways, 8 genes (RASIP1, DCN, FZD4, BMPER, CD34, TNFSF15, EDAR and ADM2) in angiogenesis, and 4 genes (DCN, FMOD, FST and SMAD6) in TGFb signaling. Importantly, modulation of metabolite pathways, anti-angiogenesis or anti-TGFb therapeutics could potentially be used to prevent THS-induced gastric tumor development.

The observation that the THS exposure-related group has a worse prognosis may also reflect the broader impact of environmental factors on cancer progression and patient survival rates. This underscores the critical importance of understanding the role of exogenous agents like THS in the molecular etiology of GC. Our findings support the need for more detailed mechanistic studies to explore how THS exposure contributes to the pathogenesis of GC and whether such an effect is a direct causation or a promoter in the process.

SPP1, also known as osteopontin or early T-lymphocyte activation 1, binds to and activates matrix metalloproteinases in tumors (Lim et al., 2012). *SPP1* is enriched in ECM-receptor interactions, which are significantly associated with the EMT pathway (Masuda et al., 2017; Reiner et al., 2017), which is consistent with the results of our enrichment pathway analysis. *TRIB3* is an important stress-responsive gene, upregulated by a variety of stimuli, and plays a vital role in processes such as apoptosis, glucose and lipid metabolism, and adipocyte differentiation (Yang et al., 2021; Dong et al., 2016). *SPP1* is overexpressed in various cancers and serves as a biomarker for predicting poor outcomes, including hepatocellular carcinoma (Wang et al., 2019), gastric cancer (Zhuo et al., 2016), ovarian cancer (Zeng et al., 2018), and glioblastoma (Chen et al., 2019). *TRIB3* regulates cell proliferation, differentiation, apoptosis, and cellular stress; it also participates in signaling pathways such as the MAPK, PI3K, NF-κB, and TGF-beta pathways (Yang et al., 2021). Silencing *TRIB3* can downregulate the expression of *VEGFA* in gastric cancer cells, thus inhibiting endothelial cell recruitment and angiogenesis, indicating that *TRIB3* overexpression is associated with tumor angiogenesis and poor prognosis in GC patients (Dong et al., 2016). Data from our PCR analysis, Western blot experiments, and public databases all suggest that *SPP1* and *TRIB3* are highly expressed in tumor tissues, and their high expression levels are indicative of poor prognosis in GC patients.

As shown in Fig. 6, The AGS colonies were very different from MGC 803 colonies. The possible explanations for such difference could be several. One is that, under THS exposure, there were different levels of upregulation of SPP1 and TRIB3 between AGS and MGC 803 cells (Fig. 4B), with changes in *TRIB3* being more marked in AGS cells. Previous studies showed that *TRIB3* may act as a cellular stress sensor (Xiao et al., 2024), which can be activated by endoplasmic reticulum unfolded protein and interact with the endoplasmic reticulum stress-related sensor HNF4α (Yu et al., 2020). Additionally, *TRIB3* regulates autophagy flux by activating the PI3K-AKT-mTOR pathway, and improves cellular stress adaptation by inhibiting ferroptosis, among other mechanisms (Chen et al., 2024; Hua et al., 2015). Also importantly, THS induces DNA damage and oxidative stress (Hang et al., 2019b; Sarker et al., 2020);. The more dramatic change in *TRIB3* in AGS cells thereby enhances their stress adaptation capabilities, leading to a more significant promotion of cell proliferation under THS exposure, as observed in our colony formation assays.

The development of GC is considered a multifactorial process involving cell proliferation, apoptosis, cellular adhesion, motility as well

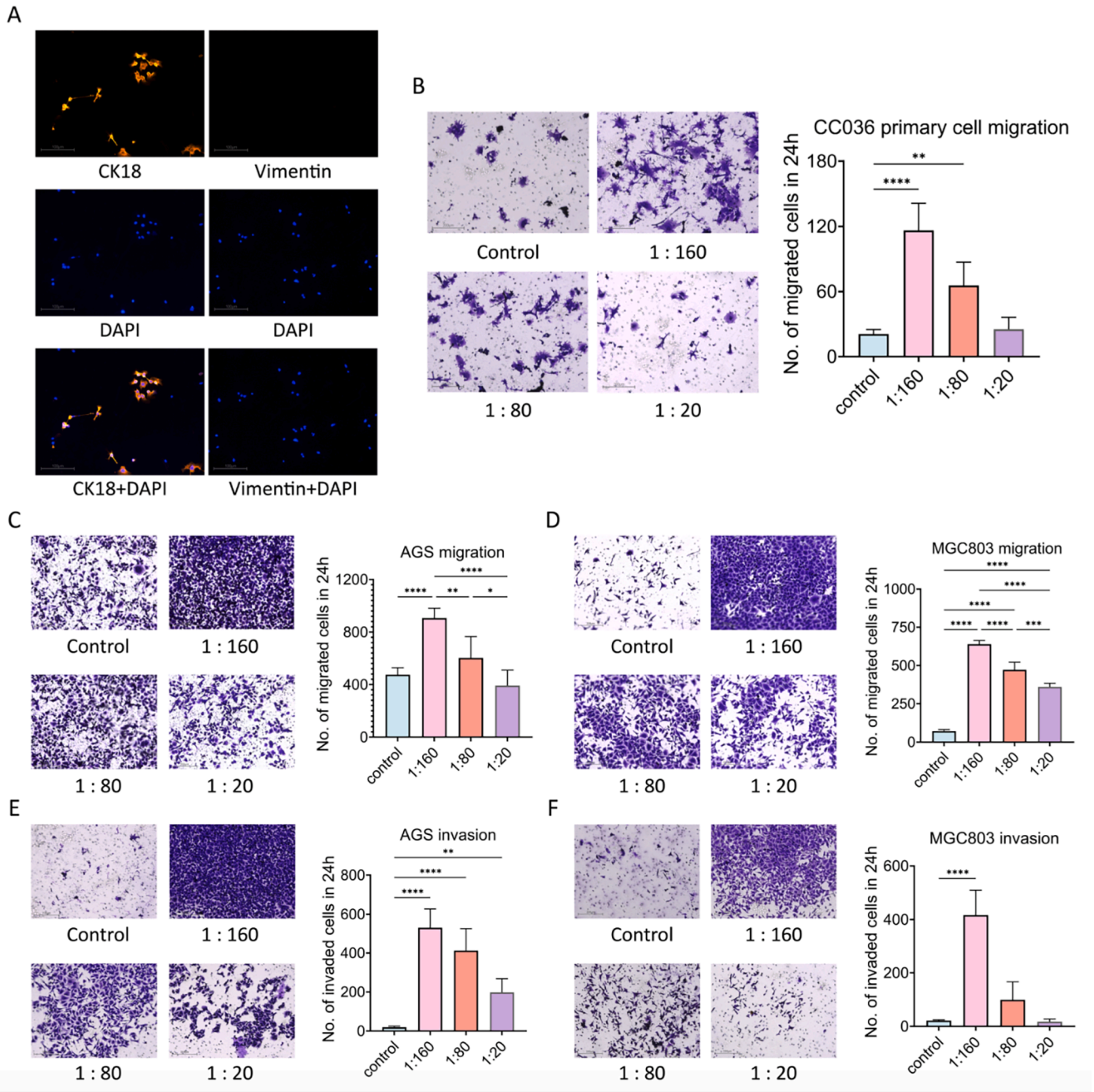

Fig. 5. Effect of THS exposure on cell migration and invasion. (A) Validation of epithelial cell identity via immunofluorescence staining of CD18+/Vimentin in extracted cells; (B) Enhanced migration of primary CC036 gastric epithelial cells upon THS exposure, without Matrigel, as visualized on the left (100 × magnification) and quantified on the right; (C-D) Increased migration of AGS and MGC803 cells under various THS concentrations, without Matrigel. (E-F) Amplified migration and invasion of AGS and MGC803 cells across Matrigel-coated membranes under THS treatment. Quantitative results are reported (mean ± SEM), with statistical significance denoted (*P<0.05, **P<0.01, ***P<0.001).

as multiple signal transduction pathways (Zhang et al., 2020; Dai et al., 2021; Han et al., 2020; Gao et al., 2020; Li et al., 2021). We employed *in vitro* experiments to observe the effects of THS exposure on the oncogenic traits of CC036 mouse gastric primary epithelial cells and human GC cell lines. As previously mentioned, our sequencing analysis revealed an enrichment of cell adhesion-related gene pathways following THS treatment; therefore, we treated both CC036 mouse gastric primary epithelial cells and human GC cell lines with varying concentrations of THS and examined migration and invasion. Our results suggest that THS exposure significantly promotes the metastatic potential of GC. We also observed that, in the AGS cell line, THS exposure significantly increased cell proliferation and enhanced anti-apoptotic capabilities. The cell migration and invasion induction of THS reduced with the exposure concentration increase, as shown in Fig. 4. This phenomenon is known as a "bell-shaped curve", which describes a situation where low to moderate doses of a substance can stimulate a biological process (such as tumor cell invasion and metastasis), but at higher doses, this effect may decrease. When the concentration increases to a certain level, the toxic effects become stronger, leading to cell death or other severe damages, which affect cell migration and invasion. In contrast, in the MGC803 cell line, no significant effect of THS exposure on cell proliferation or apoptosis was observed. This could be due to the lower sensitivity to the genetic changes described above.

EMT is characterized by a series of phenotypic changes where

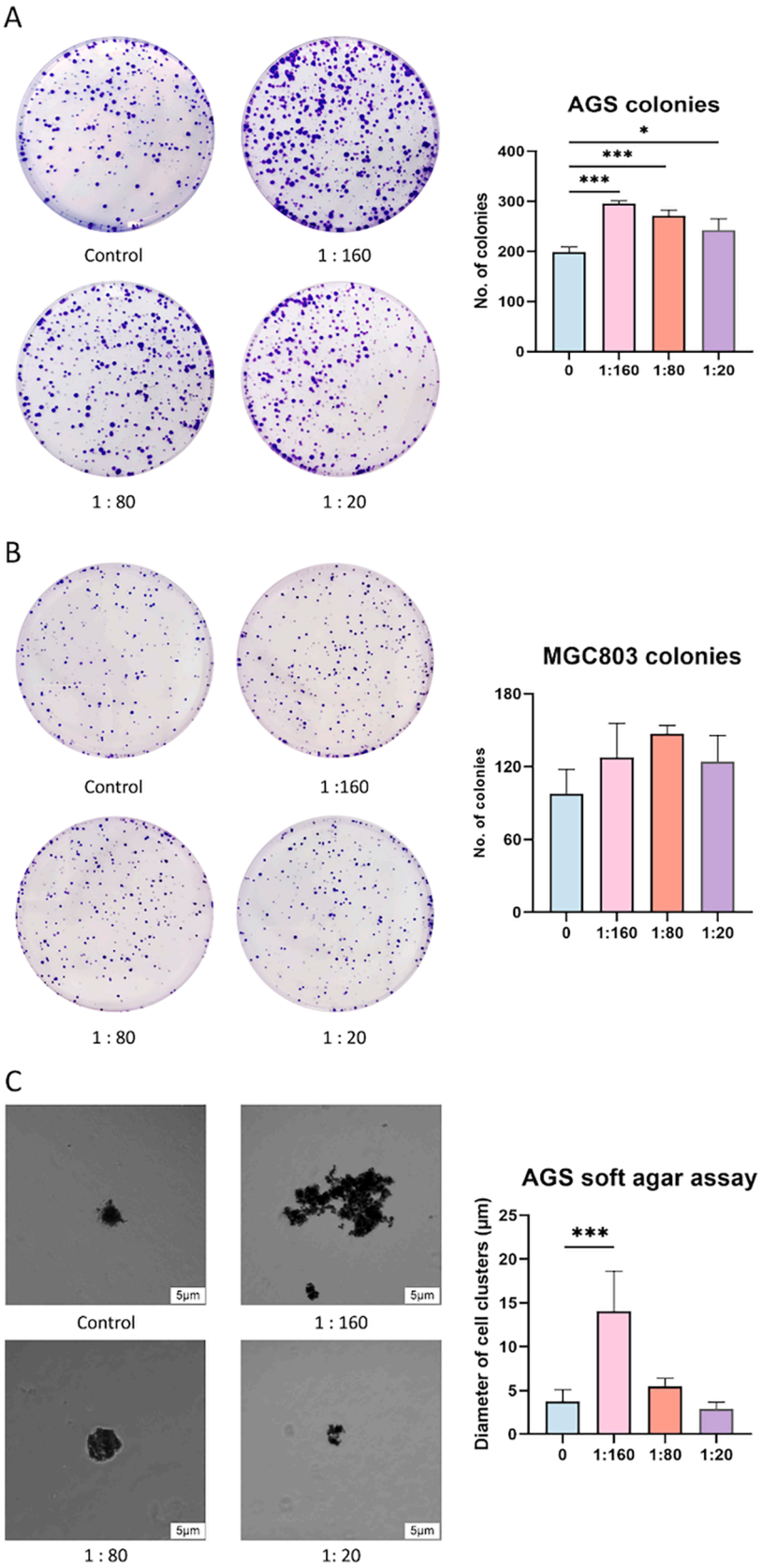

Fig. 6. Influence of THS Exposure on Cell Proliferation. (A) Augmentation of AGS cell clonogenic potential under varied THS exposures; (B) Neutral effect of THS on MGC803 cell clonogenicity. The left panel shows representative cultures, and the right panel details colony quantification (mean ± SEM, $^{*}P<0.05$, $^{**}P<0.01$, $^{***}P<0.001$); (C) THS exposure enlarges colony diameters in AGS cell soft agar cultures, with representative clusters and quantitative diameters shown (mean ± SEM from five random clusters).

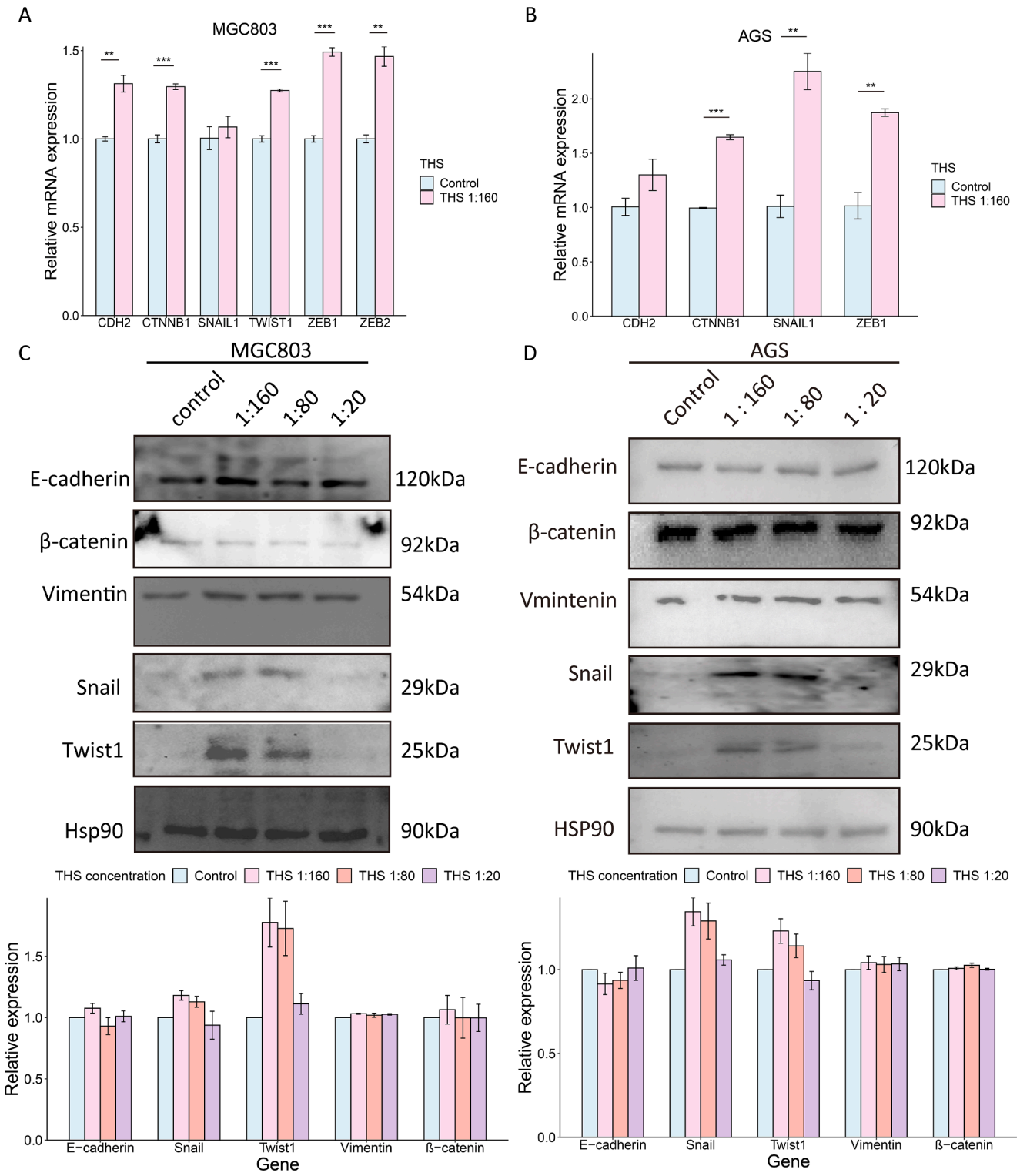

Fig. 7. THS exposure upregulated EMT marker expression in MGC803 and AGS cells. (A) Enhanced mRNA levels of EMT-related genes (*CTNNB1*, *TWIST1*, *CDH2*, *ZEB1*, *ZEB2*) in MGC803 cells following THS exposure (1:160); (B) Elevated mRNA levels of EMT markers (*CTNNB1*, *SNAI1*, *ZEB1*) in AGS cells upon THS treatment. Protein levels of EMT markers (E-cadherin, β-catenin, Vimentin, Twist1, Snail) are depicted for MGC803 (C) and AGS (D) cell lines under different THS gradients (*P<0.05, **P<0.01, ***P<0.001).

epithelial cells acquire mesenchymal features, including the dissolution of cell–cell junctions, changes in cell shape, alterations in cytoskeletal structure and adhesion molecules, production of ECM proteins, and an increase in motility and invasiveness (Chen et al., 2013). This work has demonstrated that THS exposure is associated with enrichment of genes related to the ECM pathway and the promotion of invasion in both mouse and human gastric cells. Our data from RNA sequencing analysis, together with RT-PCR and Western blot, strongly indicate that key EMT markers such as *CTNNB1*, *TWIST1*, *CDH2*, *ZEB1*, *ZEB2*, and *SNAI1* were upregulated in the samples exposed to THS. Increased expression of CTNNB1, a key component of the cadherin-catenin complex, suggests potential disruption of cell–cell adhesion, a hallmark of EMT, thus

supporting increased cell motility. Similarly, the induction of transcription factors Twist1 and Snail signifies activation of the EMT pathway, as these factors are known to suppress E-cadherin expression and promote a mesenchymal phenotype. The consistent overexpression of *ZEB1* and *ZEB2* further confirms the involvement of pathways that stimulate mesenchymal transition, typically associated with increased tumor invasiveness. The enhanced invasive and migratory capabilities shown in our *in vitro* experiments add a functional layer of evidence to the transcriptomic and proteomic findings.

In this study, we also assessed the immune microenvironment within the GC tissues of the CC036 mice and found that there was no significant difference in the infiltration of helper T cells (CD3+/CD4+), cytotoxic T cells (CD3+/CD8+), T regulatory (Treg) cells (CD4+/FoxP3+), total macrophages, M1-like macrophages, and M2-like macrophages between the THS-exposed group and the control group. Based on our previous findings in CC036 (Wang et al., 2019), it is still possible that an inflammatory response might have already created a carcinogenic microenvironment prior to the occurrence of mouse GC. THS exposure could further enhance inflammation, as observed in other systems (Matins-Green et al., 2014; Sakamaki-Ching et al., 2022), accelerating the development of cancer. Future experiments are needed to validate such a hypothesis, and it may be necessary to assess the impact of THS on the immune system at different stages of tumor development.

This study still has few limitations: First, our study focuses on the effect of THS on induction of gastric cancer in a single mouse strain, i.e., CC036, mainly because this is the only spontaneous gastric tumor model identified in Collaborative Cross mice thus far. Future studies should expand on these studies by including additional Collaborative Cross strains and other tumor endpoints in addition to gastric cancer. Second, we only observed the immune status of the CC036 mouse stomach tissues at the endpoint of our experiments. Future studies should investigate alterations of the immune microenvironment at additional timepoints during tumor development.

In summary, this study provides the first evidence that gene-environment interaction plays a critical role in the development of GC. We identified a THS exposure-induced 91-gene expression signature in CC036 and a corresponding 84-gene signature in human GC patients that predicted poorer prognosis, with *SPP1* and *TRIB3* emerging as potential targets through which THS may promote gastric carcinogenesis. THS exposure also increases *in vitro* tumorigenic traits in both mouse and human GC cells. THS exposure activates the EMT pathway, leading to overexpression and functional enrichment of ECM protein-related genes. Together, these findings offer strong evidence that THS exposure contributes to the initiation and progression of GC. In conclusion, the carcinogenic potential of THS exposure, should be acknowledged as a potential etiological factor in gastric carcinogenesis. Ultimately, knowledge of the mechanisms by which THS exposure increases the chance of disease development in exposed individuals should lead to new strategies for prevention as well as help framing and/or enforcing tobacco control policies to protect vulnerable subpopulations such as children.

CRediT authorship contribution statement

Chengfei Jiang: Visualization, Validation, Software, Methodology, Investigation, Formal analysis, Data curation. **Lingyan Chen:** Visualization, Validation, Software, Methodology, Investigation, Formal analysis, Data curation. **Chunping Ye:** Visualization, Validation, Software, Resources, Methodology, Investigation, Formal analysis, Data curation. **Suzaynn F. Schick:** Resources. **Peyton Jacob:** Resources, Formal analysis. **Yingjia Zhuang:** Investigation, Data curation. **Jamie L. Inman:** Formal analysis, Data curation. **Changbin Chen:** Validation, Software, Investigation, Formal analysis. **Lara A. Gundel:** Formal analysis, Data curation. **Hang Chang:** Validation, Software, Investigation, Formal analysis. **Antoine M. Snijders:** Writing – review & editing, Formal analysis, Data curation. **Xiaoping Zou:** Writing – original draft, Supervision, Formal analysis, Data curation, Conceptualization. **Jian-Hua Mao:** Writing – review & editing, Methodology, Investigation, Formal analysis, Data curation, Conceptualization. **Bo Hang:** Writing – original draft, Validation, Supervision, Formal analysis, Data curation, Conceptualization. **Pin Wang:** Writing – original draft, Validation, Supervision, Project administration, Funding acquisition, Formal analysis, Data curation, Conceptualization.

Declaration of competing interest

The authors declare that they have no known competing financial interests or personal relationships that could have appeared to influence the work reported in this paper.

Data availability

The RNA-seq data have been deposited at NCBI SRB under accession code BioProject: PRJNA1081597.

Acknowledgement

This work has been supported by the National Natural Science Foundation of China (ID Number: 82272952), the Natural Science Foundation of Jiangsu Province for Excellent Young Scholars (ID Number: BK20220094) and China Postdoctoral Science Foundation (ID Number: 2022M721579). This work was also partially supported by the University of California Tobacco Related Disease Research Program (UC TRDRP) (28PT-0076, 28PT-0077, 24RT-0039, 28PT-0081, T32PT6041 and T32PT6221). Laboratory resources for analytical chemistry at UCSF were supported by NIH grant P30 DA012393.

Appendix A. Supplementary data

Supplementary data to this article can be found online at https://doi.org/10.1016/j.envint.2024.108986.

References

Bahl, V., Jacob III, P., P., Havel, C., Schick, S.F., Talbot, P., 2014. Thirdhand cigarette smoke: factors affecting exposure and remediation. *PLoS One* 9, e108258.

Bahl, V., Weng, N.J., Schick, S.F., Sleiman, M., Whitehead, J., Ibarra, A., Talbot, P., 2016a. Cytotoxicity of thirdhand smoke and identification of acrolein as a volatile thirdhand smoke chemical that inhibits cell proliferation. Toxicol. Sci. 150, 234–246.

Bahl, V., Johnson, K., Phandthong, R., Zahedi, A., Schick, S.F., Talbot, P., 2016b. Thirdhand cigarette smoke causes stress-induced mitochondrial hyperfusion and alters the transcriptional profile of stem cells. Toxicol. Sci. 153, 55–69.

Bonnans, C., Chou, J., Werb, Z., 2014. Remodelling the extracellular matrix in development and disease. Nat. Rev. Mol. Cell Biol. 15 (12), 786–801.

California Environmental Protection Agency. Air Resources Board, 2005. Proposed Identification of Environmental Tobacco Smoke as a Toxic Air Contaminant... as Approved by the Scientific Review Panel on June 24, 2005: Health effects.

Chen, Q.K., Lee, K., Radisky, D.C., Nelson, C.M., 2013. Extracellular matrix proteins regulate epithelial–mesenchymal transition in mammary epithelial cells. Differentiation 86 (3), 126–132.

Chen, L., Lin, W., Zhang, H., Geng, S., Le, Z., Wan, F., Huang, Q., Chen, H., Liu, X., Lu, J. J., Kong, L., 2024. TRIB3 promotes malignancy of head and neck squamous cell carcinoma via inhibiting ferroptosis. Cell Death Dis. 15 (3), 178.

Chen, P., Zhao, D., Li, J., Liang, X., Li, J., Chang, A., Henry, V.K., Lan, Z., Spring, D.J., Rao, G., Wang, Y.A., DePinho, R.A., 2019. Symbiotic macrophage-glioma cell interactions reveal synthetic lethality in PTEN-null glioma. Cancer Cell 35 (6), 868–884.

Dai, J., Peng, T., Yu, X., 2021. NK6 homeobox 2 regulated gastrokin-2 suppresses gastric cancer cell proliferation and invasion via Akt signaling pathway. Cell Biochem. Biophys. 79, 123–131.

Dehghani, M.H., Bashardoust, P., Nayeri, D., Ghalhari, M.R., Yazdi, N.B., Jajarmi, F., 2024. A comprehensive review of the potential outcomes of exposure to tobacco smoke or secondhand smoke. Health Effects Indoor Air Pollut. 167–189.

Destaillats, H., Singer, B.C., Lee, S.K., Gundel, L.A., 2006. Effect of ozone on nicotine desorption from model surfaces: evidence for heterogeneous chemistry. Environ. Sci. Technol. 40 (6), 1799–1805.

Dong, S., Xia, J., Wang, H., Sun, L., Wu, Z., Bin, J., Liao, Y., Li, N., Liao, W., 2016. Overexpression of TRIB3 promotes angiogenesis in human gastric cancer. Oncol. Rep. 36 (4), 2339–2348.

Duan, L., Wu, A.H., Sullivan-Halley, J., Bernstein, L., 2009. Passive smoking and risk of oesophageal and gastric adenocarcinomas. Br. J. Cancer 100 (9), 1483–1485.
Gao, N., Yang, F., Chen, S., Wan, H., Zhao, X., Dong, H., 2020. The role of TRPV1 ion channels in the suppression of gastric cancer development. J. Exp. Clin. Cancer Res. 39, 1–17.
Han, X., Zhang, H.B., Li, X.D., Wang, Z.A., 2020. Long non-coding RNA X-inactive-specific transcript contributes to cisplatin resistance in gastric cancer by sponging miR-let-7b. Anticancer Drugs 31 (10), 1018–1025.
Hang, B., Lavarone, A., Havel, C., Jacob III, P., Villalta, P., Matter, B., Sharan, D., Hang, M., Sleiman, M., Destaillats, H., Gundel, LA., Chenna, A. 247th National Meeting of the American Chemical Society (ACS) with Press Release, Dallas, 2014. American Chemical Society; Washington, DC: 2014. NNA, a Thirdhand Smoke Constituent, Induces DNA Damage in Vitro and in Human Cells.
Hang, B., Sarker, A.H., Havel, C., Saha, S., Hazra, T.K., Schick, S., Jacob III, P., Rehan, V. K., Chenna, A., Sharan, D., Sleiman, M., Destaillats, H., Gundel, L.A., et al., 2013. Thirdhand smoke causes DNA damage in human cells. Mutagenesis 28, 381–391.
Hang, B., Wang, Y., Huang, Y., Wang, P., Langley, S.A., Bi, L., Sarker, A.H., Schick, S.F., Havel, C., Jacob 3rd, P., Benowitz, N., Destaillats, H., Tang, X., Xia, Y., Jen, K.Y., Gundel, L.A., Mao, J.H., Snijders, A.M., 2018. Short-term early exposure to thirdhand cigarette smoke increases lung cancer incidence in mice. Clin. Sci. (lond.) 132, 475–488.
Hang, B., Mao, J.H., Snijders, A.M., 2019a. Genetic susceptibility to thirdhand-smokeinduced lung cancer development. Nicotine Tob. Res. 21, 1294–1296.
Hang, B., Wang, P., Zhao, Y., Chang, H., Mao, J.H., Snijders, A.M., 2019b. Thirdhand smoke: Genotoxicity and carcinogenic potential. Chronic Dis. Transl. Med. 6, 27–34.
He, L., Wang, P., Schick, S.F., Huang, A., Jacob III, P., P., Yang, X., Xia, Y., Snijders, A.M., Mao, J.H., Chang, H., Hang, B., 2021. Genetic background influences the effect of thirdhand smoke exposure on anxiety and memory in Collaborative Cross mice. Sci. Rep. 11, 13285.
Hecht, S.S., 2003. Tobacco carcinogens, their biomarkers and tobacco-induced cancer. Nat. Rev. Cancer 3 (10), 733–744.
Hecht, S.S., 2012. Lung carcinogenesis by tobacco smoke. Int. J. Cancer 131 (12), 2724–2732.
Hua, F., Li, K., Yu, J.J., Hu, Z.W., 2015. The TRIB3-SQSTM1 interaction mediates metabolic stress- promoted tumorigenesis and progression via suppressing autophagic and proteasomal degradation. Autophagy 11 (10), 1929–1931.
IARC Working Group on the Evaluation of Carcinogenic Risks to Humans, World Health Organization and International Agency for Research on Cancer, 2004. Tobacco Smoke and Involuntary Smoking (Vol. 83). IARC.
IARC Working Group on the Evaluation of Carcinogenic Risks to Humans and International Agency for Research on Cancer, 2007. Smokeless Tobacco and Some Tobacco-Specific N-Nitrosamines (Vol. 89). World Health Organization.
Jacob III, P., Benowitz, N.L., Destaillats, H., Gundel, L., Hang, B., Martins-Green, M., Matt, G.E., Quintana, P.J., Samet, J.M., Schick, S.F., Talbot, P., Aquilina, N.J., Hovell, M.F., Mao, J.H., Whitehead, T.P., 2017. Thirdhand smoke: new evidence, challenges, and future directions. Chem. Res. Toxicol. 30 (1), 270–294.
Jin, X., Zhang, Y., Celniker, S.E., Xia, Y., Mao, J.H., Snijders, A.M., Chang, H., et al., 2021. Gut microbiome partially mediates and coordinates the effects of genetics on anxiety in Collaborative Cross mice. Sci. Rep. 11, 270.
Kim, Y.M., Snijders, A.M., Brislawn, C.J., Stratton, K.G., Zink, E.M., Fansler, S.J., Metz, T. O., Mao, J.H., Jansson, J.K., 2019. Light-Stress Influences the Composition of the Murine Gut Microbiome, Memory Function, and Plasma Metabolome. Front. Mol. Biosci. 6, 108.
Li, Z., Gao, H., Liu, Y., Wu, H., Li, W., Xing, Y., Zhang, Z., Zhang, X., 2021. Genetic variants in the regulation region of TLR4 reduce the gastric cancer susceptibility. Gene 767, 145181.
Li, J., Xu, H.L., Yao, B.D., Li, W.X., Fang, H., Xu, D.L., Zhang, Z.F., 2020. Environmental tobacco smoke and cancer risk, a prospective cohort study in a Chinese population. Environ. Res. 191, 110015.
Lim, A.M., Rischin, D., Fisher, R., Cao, H., Kwok, K., Truong, D., McArthur, G.A., Young, R.J., Giaccia, A., Peters, L., Le, Q.T., 2012. Prognostic significance of plasma osteopontin in patients with locoregionally advanced head and neck squamous cell carcinoma treated on TROG 02.02 phase III trial. Clin. Cancer Res. 18 (1), 301–307.
Mao, J.H., Langley, S.A., Huang, Y., Hang, M., Bouchard, K.E., Celniker, S.E., Brown, J. B., Jansson, J.K., Karpen, G.H., Snijders, A.M., 2015. Identification of genetic factors that modify motor performance and body weight using Collaborative Cross mice. Sci. Rep. 5, 16247.
Mao, J.H., Kim, Y.M., Zhou, Y.X., Hu, D., Zhong, C., Chang, H., Brislawn, C.J., Fansler, S., Langley, S., Wang, Y., Peisl, B.Y.L., Celniker, S.E., Threadgill, D.W., Wilmes, P., Orr, G., Metz, T.O., Jansson, J.K., Snijders, A.M., 2020. Genetic and metabolic links between the murine microbiome and memory. Microbiome 8, 53.
Martins-Green, M., Adhami, N., Frankos, M., Valdez, M., Goodwin, B., Lyubovitsky, J., Dhall, S., Garcia, M., Egiebor, I., Martinez, B., Green, H.W., Havel, C., Yu, L., Liles, S., Matt, G., Destaillats, H., Sleiman, M., Gundel, L.A., Benowitz, N., Jacob III, P., Hovell, M., Winickoff, J.P., Curras-Collazo, M., 2014. Cigarette smoke toxins deposited on surfaces: implications for human health. PLoS One 9, e86391.
Masuda, Y., Yokose, S., Sakagami, H., 2017. Gene expression analysis of cultured rat-endothelial cells after Nd: YAG laser irradiation by Affymetrix GeneChip Array. Vivo 31 (1), 51–54.
Matt, G.E., Quintana, P.J., Destaillats, H., Gundel, L.A., Sleiman, M., Singer, B.C., Jacob III, P., Benowitz, N., Winickoff, J.P., Rehan, V., Talbot, P., Schick, S., Samet, J., Wang, Y., Hang, B., Martins-Green, M., Pankow, J.F., Hovell, M.F., 2011. Thirdhand tobacco smoke: emerging evidence and arguments for a multidisciplinary research agenda. Environ. Health Perspect. 119 (9), 1218–1226.
Matt, G.E., Quintana, P.J.E., Hoh, E., Zakarian, J.M., Dodder, N.G., Record, R.A., Hovell, M.F., Mahabee-Gittens, E.M., Padilla, S., Markman, L., Watanabe, K., Novotny, T.E., 2021. Remediating thirdhand smoke pollution in multiunit housing: temporary reductions and the challenges of persistent reservoirs. Nicotine Tob Res. 23 (2), 364–372.
Mbemi, A., Khanna, S., Njiki, S., Yedjou, C.G., Tchounwou, P.B., 2020. Impact of gene–environment interactions on cancer development. Int. J. Environ. Res. Public Health 17 (21), 8089.
Office of the Surgeon General (US), 2004. The health consequences of smoking: a report of the Surgeon General. Atlanta (GA): Centers for Disease Control and Prevention (US).
Reiner, J., Karger, L., Cohen, N., Mehta, L., Edelmann, L., Scott, S.A., 2017. Chromosomal microarray detection of constitutional copy number variation using saliva DNA. J. Mol. Diagn. 19 (3), 397–403.
Sakamaki-Ching, S., Schick, S., Grigorean, G., Li, J., Talbot, P., 2022. Dermal thirdhand smoke exposure induces oxidative damage, initiates skin inflammatory markers, and adversely alters the human plasma proteome. EBioMedicine 84, 104256.
Sarker, A.H., Trego, K.S., Zhang, W., Jacob 3rd, P., Snijders, A.M., Mao, J.H., Schick, S.F., Cooper, P.K., Hang, B., 2020. Thirdhand smoke exposure causes replication stress and impaired transcription in human lung cells. Environ. Mol. Mutagen 61, 635–646.
Schick, S.F., Farraro, K.F., Perrino, C., Sleiman, M., van de Vossenberg, G., Trinh, M.P., Hammond, S.K., Jenkins, B.M., Balmes, J., 2014. Thirdhand cigarette smoke in an experimental chamber: evidence of surface deposition of nicotine, nitrosamines and polycyclic aromatic hydrocarbons and de novo formation of NNK. Tob. Control 23, 152–159.
Sleiman, M., Gundel, L. A., Pankow, J. F., Jacob III, P., 3rd, Singer, B. C., Destaillats, H., 2010. Formation of carcinogens indoors by surface-mediated reactions of nicotine with nitrous acid, leading to potential thirdhand smoke hazards. Proc. Natl. Acad. Sci. USA. 107(15), 6576–6581.
Snijders, A.M., Langley, S.A., Kim, Y.M., Brislawn, C.J., Noecker, C., Zink, E.M., Fansler, S.J., Casey, C.P., Miller, D.R., Huang, Y., Karpen, G.H., Celniker, S.E., Brown, J.B., Borenstein, E., Jansson, J.K., Metz, T.O., Mao, J.H., 2016. Influence of early life exposure, host genetics and diet on the mouse gut microbiome and metabolome. Nat. Microbiol. 2, 16221.
Steevens, J., Schouten, L.J., Goldbohm, R.A., Van den Brandt, P.A., 2010. Alcohol consumption, cigarette smoking and risk of subtypes of oesophageal and gastric cancer: a prospective cohort study. Gut 59, 39–48.
Tang, X., Benowitz, N., Gundel, L., Hang, B., Havel, C.M., Hoh, E., Jacob Iii, P., Mao, J.H., Martins-Green, M., Matt, G.E., Quintana, P.J.E., Russell, M.L., Sarker, A., Schick, S. F., Snijders, A.M., Destaillats, H., 2022. Thirdhand exposures to tobacco-specific nitrosamines through inhalation, dust ingestion, dermal uptake, and epidermal chemistry. Environ. Sci. Technol. 56, 12506–12516.
Wang, J., Hao, F., Fei, X., Chen, Y., 2019a. SPP1 functions as an enhancer of cell growth in hepatocellular carcinoma targeted by miR-181c. Am. J. Transl. Res. 11 (11), 6924.
Wang, P., Wang, Y., Langley, S.A., Zhou, Y.X., Jen, K.Y., Sun, Q., Brislawn, C., Rojas, C. M., Wahl, K.L., Wang, T., Fan, X., Jansson, J.K., Celniker, S.E., Zou, X., Threadgill, D. W., Snijders, A.M., Mao, J.H., 2019b. Diverse tumour susceptibility in Collaborative Cross mice: identification of a new mouse model for human gastric tumourigenesis. Gut 68, 1942–1952.
Welsh, C.E., Miller, D.R., Manly, K.F., Wang, J., McMillan, L., Morahan, G., Mott, R., Iraqi, F.A., Threadgill, D.W., de Villena, F.P.M., 2012. Status and access to the Collaborative Cross population. Mamm. Genome 23, 706–712.
Whitehead, T.P., Havel, C., Metayer, C., Benowitz, N.L., Jacob III, P., 2015. Tobacco alkaloids and tobacco-specific nitrosamines in dust from homes of smokeless tobacco users, active smokers, and nontobacco users. Chem. Res. Toxicol. 28 (5), 1007–1014.
Xiao, M.C., Jiang, N., Chen, L.L., Liu, F., Liu, S,Q., Ding, C.H., Wu, S.H., Wang, K.Q., Luo, Y,Y., Peng, Y., Yan, F.Z., Zhang, X., Qian, H., Xie, W.F., 2024. TRIB3-TRIM8 complex drives NAFLD progression by regulating HNF4α stability. J. Hepatol. 80(5): 778-791.
Yang, J., Lin, J., An, J., Zhao, Y., Jing, S., Yu, M., Zhu, Y., Yao, Y., 2021. TRIB3 promotes the malignant progression of bladder cancer: an integrated analysis of bioinformatics and *in vitro* experiments. Front. Genet. 12, 649208.
Yang, H., Wang, X., Wang, P., He, L., Schick, S.F., Jacob 3rd, P., Benowitz, N., Gundel, L. A., Zhu, C., Xia, Y., Inman, J.L., Chang, H., Snijders, A.M., Mao, J.H., Hang, B., 2023. Thirdhand tobacco smoke exposure increases the genetic background-dependent risk of Pan-tumor development in collaborative cross mice. Environ. Int. 174, 107876.
Yu, J.J., Zhou, D.D., Yang, X.X., Cui, B., Tan, F.W., Wang, J., Li, K., Shang, S., Zhang, C., Lv, X.X., Zhang, X.W., Liu, S.S., Yu, J.M., Wang, F., Huang, B., Hua, F., Hu, Z.W., 2020. TRIB3-EGFR interaction promotes lung cancer progression and defines a therapeutic target. Nat Commun. 11 (1), 3660.
Zeng, B., Zhou, M., Wu, H., Xiong, Z., 2018. SPP1 promotes ovarian cancer progression via Integrin β1/FAK/AKT signaling pathway. OncoTargets Therapy 1333–1343.
Zhang, Z., Li, Z., Zhang, X., Ye, W., Chen, J., Wang, L., Lin, Z., Li, J., Li, Z., 2023. Association between secondhand smoke and cancers in adults in the US population. J. Cancer Res. Clin. Oncol. 149 (7), 3447–3455.
Zhang, H., Wang, Y., Wang, Y., Wu, D., Lin, E., Xia, Q., 2020. Intratumoral and intertumoral heterogeneity of HER2 immunohistochemical expression in gastric cancer. Pathology-Res. Practice 216 (11), 153229.
Zhuo, C., Li, X., Zhuang, H., Tian, S., Cui, H., Jiang, R., Liu, C., Tao, R., Lin, X., 2016. Elevated THBS2, COL1A2, and SPP1 expression levels as predictors of gastric cancer prognosis. Cell. Physiol. Biochem. 40 (6), 1316–1324.